Analysis of random telegraph noise in large-area amorphous double-barrier structures

T. Teuschler, M. Hundhausen, and L. Ley
Institut für Technische Physik, Universität Erlangen-Nürnberg, Erwin-Rommel-Straße 1, W-8520 Erlangen, Federal Republic of Germany

R. Arce
Instituto de Desarrollo Tecnológico para la Industria Química, Güemes 3450, 3000 Santa Fe, Argentina
(Received 19 May 1992)

We have measured the temporal behavior of the perpendicular current through large-area (≈ 0.25 mm^2) double-barrier structures fabricated from n^+-type a-Si:H and quasistoichiometric a-SiN_x:H. The current switches randomly between distinct values with an amplitude between 0.5% and 10% of the total current. This behavior is reminiscent of random telegraph noise (RTN) observed in small-area (< 1 μm^2) devices. The power spectra of the RTN can be fitted by a superposition of Lorentzians from which effective switching rates can be deduced. They are thermally activated and exhibit a dependence on the voltage applied to the sample. The RTN switching can be influenced optically by illuminating the sample surface with a He-Ne laser. While scanning the device area with the focused laser the RTN is influenced at one well-defined spot only. We associate this spot with a filament of less than 1 μm^2 in size that carries a large fraction of the current through the device and argue that the current is controlled by the charging and discharging of a single defect in proximity to this filament via Coulomb blocking resulting in the observed RTN. In different samples distributions of switching times for capture and emission of electrons at a single defect are measured as a function of applied voltage and temperature. Based on these data different configurations of the defect located in the nitride barrier are discussed within a model of an acceptorlike trap with a strong electron-lattice coupling which exchanges charge with the adjacent n^+-type a-Si:H layers.

I. INTRODUCTION

The statistical switching of the electrical resistance of a device between two discrete values is termed "random telegraph noise (RTN)" because the current through such a device resembles a telegraph signal. One of the first reports of RTN dates back to the 1960s when Wolf and Holler observed RTN in the current through reverse biased Ge p-n junctions.[1] Since then RTN has been observed in a wide variety of devices. Examples range from metal-oxide-semiconductor (MOS) capacitors[2] and quantum well diodes[3] over metallic point contacts[4,5] to the current in a scanning tunneling microscope where the tip is kept fixed over an oxidized Si surface.[6] In amorphous silicon samples RTN was observed in devices based on rf-sputtered a-Si:H,[7,8] as well as on glow-discharge a-Si:H.[9,10] By far, the most studied devices showing RTN are, however, field-effect transistors (FET's),[11–21] where the characteristic switching occurs in the source-drain current.

There is mounting evidence that RTN is caused by the statistical discharging and charging of individual defects that control the device resistance by blocking the current-carrying path through the device by their Coulomb field. It is obvious that an analysis of the switching times thus affords a unique opportunity to study the occupation kinetics of an individual trap, information that is not accessible with any other technique. Moreover, it has been shown that the ubiquitous $1/f$ noise may be considered as due to the superposition of RTN from many traps with a wide distribution of switching times.[19]

A necessary condition for measurable resistance changes in the form of RTN to occur is that the dimensions of the current-carrying path are comparable to the screening length of the trapped charge. Therefore, RTN is generally observed in submicrometer devices where this condition is met.

It thus came as somewhat of a surprise to us to observe RTN in the current through amorphous double-barrier structures (DBS) of typically 0.25-mm^2 cross-sectional area.[22,23] An analysis of the effective switching rates in terms of their spectral power density and as a function of temperature and applied voltage showed great similarity with features characteristic for RTN in small-area devices. We therefore postulated that the current through our devices was effectively restricted to a filament of submicrometer dimension due to lateral variations in the barrier width where a single trap could control the resistance of the device. In this contribution we shall present—among other things—direct evidence that this conjecture was correct.

The paper is organized as follows. After a brief description of some experimental details and a review of our earlier work on RTN in large-area DBS we shall present evidence for a confinement of the current-carrying filament to a fraction of the actual sample area. We proceed by analyzing the distribution of switching times in the high- and low-current states as a function of applied voltage and temperature and derive models for

 ©1993 The American Physical Society

the microscopic charging and discharging kinetics of the traps responsible for RTN.

II. EXPERIMENTAL DETAILS

The samples for this investigation consist of a 40-Å-thick n^+-type a-Si:H well enclosed by two 40-Å-thick a-SiN_x:H barriers. This structure is sandwiched between the two 500-Å-thick n^+-type a-Si:H layers (see Fig. 1). Samples were deposited by rf-glow-discharge techniques described elsewhere[25] on quartz substrates covered with chromium which also served as the bottom contact. The n^+-type a-Si:H layers were deposited from a mixture of 1% PH_3 in SiH_4, and for the a-SiN_x:H barriers we used 12.5% SiH_4 diluted in NH_3. This resulted in quasistoichiometric SiN_x:H, i.e., $x=\frac{4}{3}$, with an optical gap of about 3.9 eV. In order to obtain sharp interfaces between the layers a shutter was used to avoid deposition of material during a changeover from one gas mixture to the other. After deposition regular arrays of semitransparent Cr contacts were evaporated on top of the samples to define devices with cross-sectional areas between 500×500 and 2000×2000 μm^2. A schematic band diagram of the finished devices with band offsets according to Ref. 24 is also shown in Fig. 1.

We mention in passing that these structures were originally built to confirm the report of resonant tunneling in similar devices by Miyazaki, Ihara, and Hirose,[26] albeit with negative results.

The noise characteristics of our samples were measured in the constant-voltage mode using a battery-powered voltage source and a low-noise current preamplifier. After appropriate filtering and subtraction of a constant-current offset, the temporal current fluctuations were recorded with a digital storage oscilloscope and read periodically into a computer for further treatment. The accessible frequency range was from 0.02 Hz to 25 kHz. The intrinsic noise contributions of the electronics to the spectral power density of the current fluctuations were measured after replacing the sample by a metal film resistor of equivalent impedance to be less than 2×10^{-24} A^2/Hz between 1 and 10^3 Hz and below 2×10^{-23} A^2/Hz below 1 Hz, i.e., they were negligible in the current context. The temperature of the sample mounted in an optical cryostat could be controlled in the range between 100 and 400 K during measurements.

III. RESULTS

A. Analysis of the RTN spectra

In Fig. 2 we show a typical I/U curve taken at 108 K for one of the DBS's. No particular feature in this curve is observed that could be attributed to the resonant tunneling as described in Ref. 26. Instead, we observe an I/U curve characteristic for sequential tunneling through the nitride barriers, i.e., a current that rises exponentially with applied voltage U.

The average current $\langle I\rangle$ through all the DBS's is thermally activated. The activation energy of 0.2 eV is identical to that in n^+-type a-Si:H bulk material with equivalent doping. We therefore conclude that the current through our samples is carried by electrons at the a-Si:H conduction-band edge which tunnel sequentially through both nitride barriers. From the dI/dU curve also shown in Fig. 2 the onset of excessive noise at about 0.4 V for this sample can be seen.

When plotted as a function of time, the random switching of the sample current between two distinct levels is observed as shown for an applied voltage of 0.5 V in the inset of Fig. 2. This RTN is thus characterized by the amplitude ΔI and by the distribution of times τ_0 and τ_1 during which the sample remains in its low-current (i.e., high-resistance) and high-current (i.e., low-resistance) states, respectively. We observe relative changes in current, $\Delta I/I$, that vary between 0.5% and 10% depending on the monitored trap and on the sample. Depending on the sample temperature and on the applied voltage

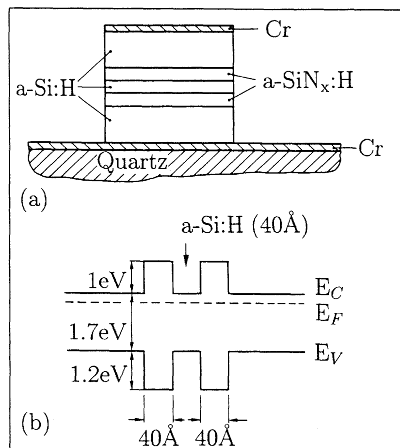

FIG. 1. (a) Schematic diagram of our double-barrier structures deposited on a quartz substrate. (b) The corresponding band diagram with band offsets according to Ref. 24.

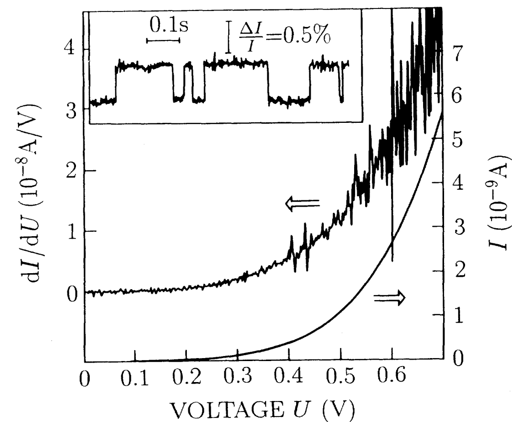

FIG. 2. Current-voltage characteristics for sample 230-1 taken at 108 K. Also plotted is the derivative of the current with respect to the voltage showing the onset of the excessive noise at about 0.4 V for this specific sample. The inset shows the current as a function of time taken at a voltage of $U=0.5$ V applied to the sample.

different noise characteristics are observed. Also, different samples show different noise behaviors.

In most of our samples more than one switching process contributes to the RTN at a given temperature and a given applied voltage. As an example, consider the time spectrum of sample 230-6 shown in the inset of Fig. 3 where three different resistance levels are observed in the time window shown.

Following common practice we analyze the RTN in terms of its spectral power density $S(f)$.[27] $S(f)$ is defined through the Fourier transform $X(f)$ of the fluctuating current $I(t)$ as

$$S(f)=\lim_{t_{\rm obs}\to\infty}\frac{2|X(f)|^2}{t_{\rm obs}}\;, \tag{1}$$

where f is the frequency and $t_{\rm obs}$ is the total time interval during which the noise signal is analyzed.

Assuming ergodicity, $S(f)$ can be estimated at the frequency f_n by fast-Fourier transformation of the current signal $I(t)$ sampled within z oscilloscope traces with N data points per trace,[28]

$$S(f_n)\approx\begin{cases}\dfrac{1}{N\Delta t}\overline{|\Delta t X_0|^2}\;, & n=0\\[2mm] \dfrac{1}{N\Delta t}\overline{|\Delta t X_n|^2+|\Delta t X_{N-n}|^2}\;, & n=1,\ldots,\dfrac{N}{2}-1\\[2mm] \dfrac{1}{N\Delta t}\overline{|\Delta t X_{N/2}|^2}\;, & n=\dfrac{N}{2}\;.\end{cases} \tag{2}$$

Here, X_i is the ith discrete Fourier transform of the N sampling points separated by the time interval Δt. The bars denote an "ensemble average" over z time traces. Typical values are $N=4096$ and $30\le z\le 300$.

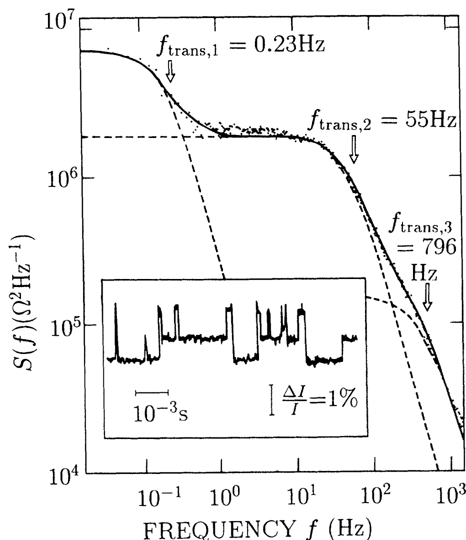

FIG. 3. Power spectral density $S(f)$ of the current noise for sample 230-6. Three different Lorentzian contributions were identified and are shown as dashed lines with their respective transition frequencies $f_{{\rm trans},i}$ that are marked with arrows. The two faster switching processes are readily identified in the current trace shown in the inset.

If capture and emission probabilities which lead to the observed RTN obey Poisson statistics, the spectral power density is directly related to the average times $\bar\tau_0$ and $\bar\tau_1$ spent in the high- and low-resistance states, respectively, and to the switching amplitude ΔI via the following Lorentzian relationship:[29]

$$S(f)=\frac{4(\Delta I)^2}{(\bar\tau_0+\bar\tau_1)[(2\pi f_{\rm trans})^2+(2\pi f)^2]}\;. \tag{3}$$

Here, $f_{\rm trans}=(2\pi)^{-1}(\bar\tau_0^{-1}+\bar\tau_1^{-1})$ is the transition frequency. It corresponds to a value of f where $S(f)$ has dropped to half its maximum value. A total of three such Lorentzians is sufficient to fit, for example, the spectral power density of Fig. 3 with transition frequencies $f_{\rm trans}$ of 0.23, 55, and 796 Hz, respectively. The slowest of these switching processes was not active during the time window while the current trace in the inset of Fig. 3 was taken; the two faster processes are readily identified.

The use of the transition frequency $f_{\rm trans}$ instead of the individual average times $\bar\tau_0$ and $\bar\tau_1$ implies, in general, a loss of information since a given $f_{\rm trans}$ can be realized with a variety of $\bar\tau_0$ and $\bar\tau_1$.

Under the conditions which lead to expression (3) for $S(f)$, the individual transition probabilities p_0 and p_1 are expected to be distributed exponentially by[19]

$$p_{0,1}=(\bar\tau_{0,1})^{-1}\exp(-\tau_{0,1}/\bar\tau_{0,1})\;. \tag{4}$$

Here, p_1 refers to the probability per unit time that the RTN stays in the high-current state 1 for a time τ_1 and then switches into the low-current state 0 and vice versa for p_0. The exponential distribution of residence times τ_0 and τ_1 is nicely borne out by the data of Fig. 4 where we show the frequency distribution of τ_0 and τ_1 for a particular sample on a semilogarithmic plot. The slopes give the time constants $\bar\tau_0=0.023$ s and $\bar\tau_1=0.163$ s corresponding to the mean times spent in the low- and high-current states, respectively. The same procedure is adopted whenever we quote time constants $\bar\tau_0$ and $\bar\tau_1$ in what follows.

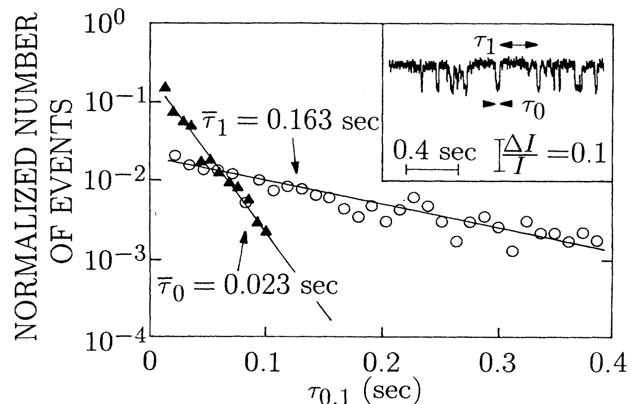

FIG. 4. Distributions of down (τ_0) and up (τ_1) times of a RTN as shown in the inset. The solid lines are least-square fits to determine the time constants $\bar\tau_0$ and $\bar\tau_1$, respectively.

B. Location of the current path

As mentioned in the Introduction the original contention concerning the manifestation of RTN in our comparatively large-area devices was that most of the current is effectively constricted to a submicrometer cross section due to lateral variations in the width of one of the barriers. We shall now demonstrate that this picture is correct utilizing the effect of light on the RTN.

When a sample that shows RTN in the dark is illuminated with light from a defocused 10-mW He-Ne laser with an intensity of 6×10^9 photons $\mathrm{s}^{-1}\,\mu\mathrm{m}^{-2}$, the current switching disappears and the spectral power density changes from its Lorentzian shape characteristic for RTN to a spectrum that is more reminiscent of the common $1/f$ power density (compare Fig. 5). Even without a detailed explanation for this behavior we use the quantity

$$\delta=\frac{S(f_{\mathrm{trans}})|_{\mathrm{dark}}}{S(f_{\mathrm{trans}})|_{\mathrm{illum}}}\,, \tag{5}$$

i.e., the change in the spectral power density at the transition frequency f_{trans} of the RTN without illumination as a measure of the influence of light on the RTN.

With a laser beam focused to a diameter of 10 μm a spatially resolved scan for a light-sensitive spot on the sample was performed. The result is shown in Fig. 6. For an illumination intensity above 1.3×10^8 photons $\mathrm{s}^{-1}\,\mu\mathrm{m}^{-2}$ the parameter δ increases sharply at one particular spot on the sample. A fit of the data points to a Gaussian profile reveals a full width at half maximum (FWHM) of 10 μm. If we assume that the spatial response of the RTN to illumination is given by a convolution of the current path profile with the Gaussian intensity profile of the probing laser of about 10-μm diameter we can conclude that the laser beam diameter is an upper limit for the spatial extent of the current path.

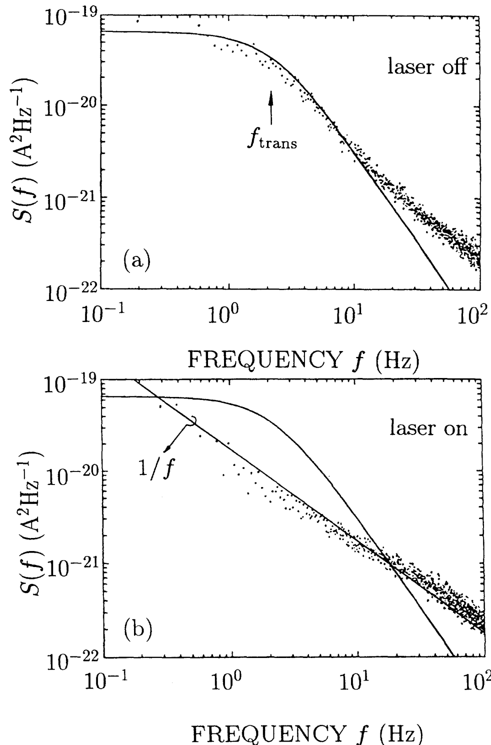

FIG. 5. (a) Spectral power density $S(f)$ measured in the dark. The solid line is a Lorentzian fit with $f_{\mathrm{trans}}=2.2$ Hz. Deviations at higher frequencies are due to additional noise around the high- and low-current states, respectively. (b) Spectral power density under illumination with 6×10^9 photons $\mathrm{s}^{-1}\,\mu\mathrm{m}^{-2}$. Note that the noise spectrum does not follow the Lorentzian dependence (RTN), which is also shown as a reference, but can be well fitted by a $1/f$ dependence.

A thermal effect of the focused laser beam on the switching process can be excluded. Using a formalism due to Lax[30] we estimate that the surface temperature of the sample at the center of the laser beam increases by no more than 0.2 K for illumination intensities where the RTN vanishes. By varying the temperature in a controlled manner we could not find a significant change in RTN for such a small temperature difference.

A further indication that the current is constricted to the light-sensitive area is given in Fig. 7 where spatially resolved measurements of the net photocurrent while scanning the sample surface are shown. Only in the region where δ increases does the sample exhibit a significant increase in photoconductivity. We thus associate the light-sensitive spot with a filament of less than 10-μm diameter that carries a large fraction of the current through the device.

Aside from a direct confirmation of the current path model the effect of light on the occupation statistics of the trap responsible for RTN offers a new access to the microscopic mechanism of capture and release of charge carriers at the site of a single trap. We shall return to this aspect in Sec. IV.

C. Temperature and voltage dependence of switching times

In our earlier investigations we had shown that the effective switching times decrease strongly with temperature, a behavior that could well be described by thermally

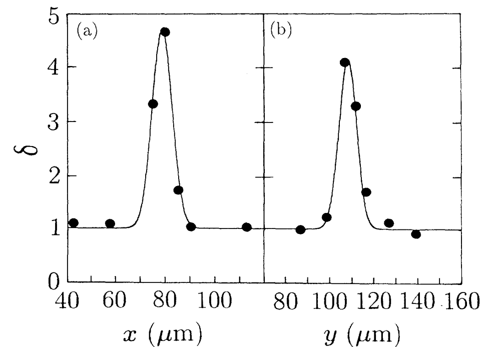

FIG. 6. Spatially resolved measurement of $\delta=S(f_{\mathrm{trans}})|_{\mathrm{dark}}/S(f_{\mathrm{trans}})|_{\mathrm{illum}}$ for trap T_1 ($f_{\mathrm{trans}}=2.2$ Hz); x and y are two perpendicular directions on the sample surface. The solid line is a fit to a two-dimensional Gaussian with a full width at half maximum (FWHM) equal to the laser beam diameter $w=10\,\mu$m.

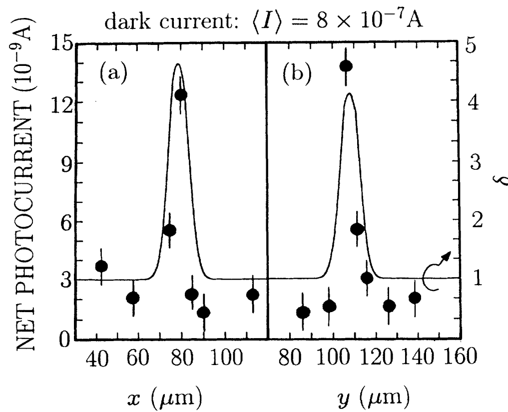

FIG. 7. Spatially resolved measurement of the net photocurrent; x and y are two perpendicular directions on the sample surface. For comparison the spatially resolved behavior of δ is also shown by a solid line. Note that an increase in photoconductivity is observed only in the region where δ increases.

activated effective switching rates $(\overline{\tau}_0^{-1}+\overline{\tau}_1^{-1})$ with activation energies between about 0.2 and 0.6 eV and prefactors in the range of 10^{10} to 10^{14} s^{-1}. It was further shown that these activation energies change with applied voltage resulting in a pronounced dependence of the effective switching rate on the applied voltage for a given temperature T.[22,23]

The analysis of the distribution of the individual times τ_1 and τ_0 performed here gives a more refined picture of the effect of temperature and applied voltage on the kinetics underlying the current switching process. In anticipation of a microscopic model, to be presented later, and for greater ease of discussion we shall identify τ_1 as the time the sample remains in its high-current, i.e., low-resistance state, with the capture time τ_c and τ_0 with the emission time τ_e of the current-controlling trap state T.

In Fig. 8 we show the average capture and emission time constants for a trap in sample 230-D2—denoted as T_1 in the following—as a function of temperature in an Arrhenius plot. As can be seen from Fig. 8 the emission time constant $\overline{\tau}_e$ decreases exponentially with temperature according to $\overline{\tau}_e=\overline{\tau}_{e0}\exp(\Delta E_{\mathrm{em}}/kT)$ with an activation energy $\Delta E_{\mathrm{em}}=(0.87\pm0.05)$ eV. Similarly, we find from Fig. 8 that the capture time constant $\overline{\tau}_c$ for T_1 is thermally activated as well with an activation energy of $\Delta E_{\mathrm{cap}}=(0.72\pm0.05)$ eV.

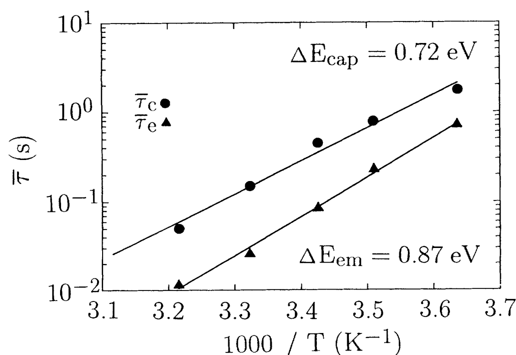

FIG. 8. $\overline{\tau}_c$ and $\overline{\tau}_e$ as a function of $1/T$ for trap T_1 in sample 230-D2. The activation energies for the capture and emission processes derived from the Arrhenius plot are indicated.

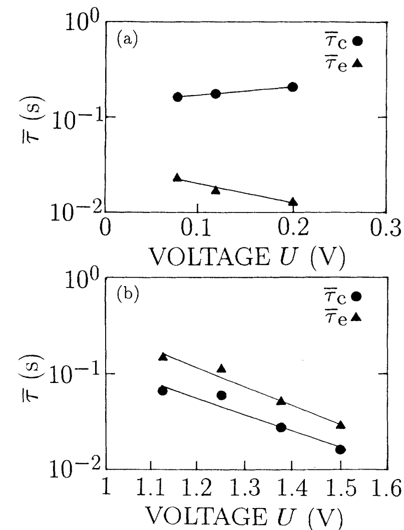

FIG. 9. $\overline{\tau}_c$ and $\overline{\tau}_e$ as a function of applied voltage for two different trap states. Note that the capture time constants show a different behavior with increasing voltage.

The thermal activation of the emission time constants $\overline{\tau}_e$ and of the capture time constants $\overline{\tau}_c$ is a generally observed phenomenon in our samples. However, the values that we obtain differ for different traps. Typical values for ΔE_{em} are 0.4–0.9 eV and 0.4–0.7 eV for ΔE_{cap}.

We have also investigated the relationship between the voltage U applied to the sample and capture and emission time constants for a number of RTN signals. The behavior of two representative traps termed T_2 and T_3 in the following are shown in Fig. 9. For T_2 [compare Fig. 9(a)] the capture time constant $\overline{\tau}_c$ increases and the emission time constant $\overline{\tau}_e$ decreases when the voltage U applied to the sample is raised. For T_3 [Fig. 9(b)] $\overline{\tau}_e$ and $\overline{\tau}_c$ both decrease with increasing voltage U.

For trap T_2 we have also measured the temperature dependence of the emission and capture time constants $\overline{\tau}_e$ and $\overline{\tau}_c$ as a function of applied voltage U. The corresponding activation energies are summarized in Table I, together with other experimental details for three traps, T_1–T_3.

IV. DISCUSSION

The identification of a current path of less than 10-μm diameter puts our original contention of a single trap to control the resistance of the DBS on firmer ground. The Coulomb potential associated with the charged trap assumed to be situated in or close to the nitride layer will locally raise the tunneling barrier and thereby decrease the tunneling current through the device. The majority carriers in our n^+-type a-Si:H–based sandwich structures are electrons. This implies that the high-resistance state corresponds to a trap occupied with an electron and

the low-resistance state to the empty trap. The corresponding times are therefore identified with the emission and capture times of the trap, respectively, as mentioned earlier.

In order to quantify the ensuing resistance changes we make a number of simplifying assumptions, the main one being that the Coulomb potential of the charged trap is only weakly disturbed by the presence of the a-Si:H/a-SiN_x interface. The blocking potential is given approximately by that of a point charge e in a medium with an effective dielectric constant $\langle \varepsilon \rangle$: $\phi(r)=e/4\pi\varepsilon_0\langle \varepsilon \rangle r$ superimposed on the band diagram of Fig. 1. Analytical solutions for a geometry with one interface indeed show that the potential is only weakly disturbed by the interface[31] and may well be approximated by an isotropic Coulomb potential using an effective $\langle \varepsilon \rangle = 8.1$. The superposition of the potential of the charged trap with the band diagram of the double-barrier structure locally distorts both barrier height and barrier width.

Next, we assume, following common practice, that a band distortion in excess of kT/e effectively blocks the current and thus reduces the cross section of the current path by an amount $Q_0 = \pi R_0^2$ with the blocking radius R_0 given by $e^2/4\pi\varepsilon_0\langle \varepsilon \rangle kT = 0.007$ μm at room temperature. This estimate holds as long as the current-controlling trap is in or close to (on the scale of R_0) the SiN_x barrier layer. At room temperature and for the observed relative current changes $\Delta I/I$ of typically 1% this means that the current path has a diameter of about 0.14 μm if the total current flows through one filament. This value is compatible with the upper limit for this diameter determined from the laser experiments of Sec. III B.

In order to observe RTN one or at most a few traps should be "active" in the current path. This limits the tolerable concentration of deep defects even if we take into account the fact that only a fraction of the total defects may be active in the sense that their switching frequency lies in the experimentally accessible range.

Let us assume that only one active trap should be situated within a cylindrical current path through one nitride barrier. The path volume is then given by the barrier width of 40 Å times a filament cross section of 1.5×10^{-10} cm^2 corresponding to an observed resistance change of 1%. This yields a tolerable defect concentration of about 1.6×10^{16} cm^{-3}. Typical defect densities of 10^{16}–to 10^{17} cm^{-3} have been reported in electron spin resonance measurements for near-stoichiometric a-SiN_x:H.[32–37]

Alternatively, if the active defects were all located at the a-Si:H/a-SiN_x:H interface an interface defect density of about 6.5×10^9 cm^{-2} would be required for a switching amplitude of about 1%. This number is smaller than defect concentrations of $\approx 10^{12}$ cm^{-2} observed in capacitance-voltage (CV) experiments for this interface,[38,35] albeit on account of the large uncertainty in our estimates we cannot preclude interface defects as the active centers based on the concentration argument alone. Supporting evidence for bulk silicon nitride traps as the active centers will be given below.

A common characteristic of the switching times in RTN signals is the fact that they are thermally activated with a wide range of activation energies.[19] Whereas an activated emission of a charge from a defect level to the nearest band edge with activation energies from zero to half the band gap depending on the position of the level will be readily accepted it is the activated nature of the capture rates that require additional assumptions about the microscopic mechanisms responsible for the charge exchange between trap and band states. Two models have been put forward to account for both activation energies.

In the model of strong electron-lattice coupling[39,40] the activation energies are associated with barriers that separate the two different equilibrium configurations of the charged and neutral traps, respectively (compare Fig. 10). This model is appealing for traps in disordered materials such as the gate oxide in MOS-FET's and the system at hand where the flexibility of the amorphous network favors strong electron-lattice coupling.

The thermionic emission model was developed by Karmann and Schulz[41] to explain RTN in small channel FET's. Here, the active trap is situated in the gate oxide and communicates with the charge in the channel via thermionic emission over a barrier which results from the superposition of the trap potential and the conduction-band discontinuity between gate oxide and channel silicon. This concept was developed into a phenomenological model which accounts nicely for most of the observed effects. The model, however, explicitly excludes a tunneling transport perpendicular to the channel. Our own data on the time constants in amorphous DBS's add a new aspect—the voltage dependence of the time constants—which require new elements to be added to the current models.

We base our discussion on a strong electron-lattice coupling to account for the activation energies because this appears to be the more general one. We can, furthermore, by no means exclude the perpendicular tunneling transport as the total current through our devices relies

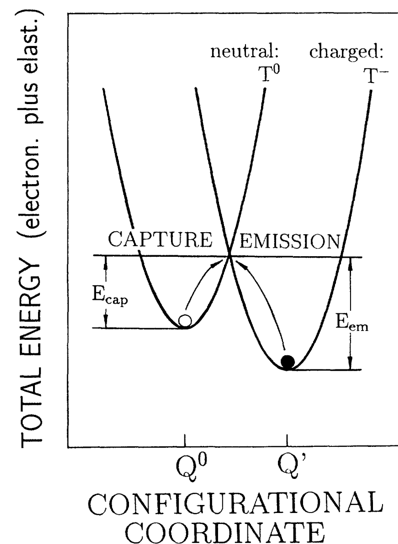

FIG. 10. Schematic configuration diagram for a trap in its neutral (T^0) and charged states (T^-). For details see text.

on electron tunneling through the nitride barriers.

The elements of our model are as follows.

(i) The active trap has two geometrically different environments, designated by generalized configurational coordinates Q_0 and Q', respectively, in Fig. 10, depending on its charge state [neutral-empty (T^0), negatively charged occupied (T^-)]. The parabola labeled T^0 in Fig. 10 represents the total (lattice + electronic) energy surfaces of the empty trap plus a "free" electron at the *a*-Si:H conduction-band edge as a function of lattice distortion Q in the harmonic approximation. The parabola T^- represents accordingly the total-energy surface of the occupied trap. The "deformation" barrier accounts[42] (up to an entropy term) for the thermally activated nature of the capture and emission time constants, respectively.

In this model the activation energy $\Delta E_{\rm em}$ for the emission time constant equals the enthalpy of the configurational barrier $E_{\rm em}$ for the transition $T^- \to T^0$. The activation energy $\Delta E_{\rm cap}$ for the capture rates, however, involves in addition to the enthalpy of the configurational barrier $E_{\rm cap}$ the thermal activation of electrons in n^+-type *a*-Si:H with a measured activation energy of 0.2 eV as stated above.

(ii) For a trap inside one of the barriers and not at one of the interfaces its energy relative to both *a*-Si:H conduction-band edges varies with the applied voltage U. It is lowered by $(eU/2)(d/t)$ with respect to the "upstream" edge and raised by $(eU/2)(t-d/t)$ relative to the "downstream"-lying conduction-band edge of the adjacent n^+-type *a*-Si:H layer where d and t are the distance to the corresponding edge and the total barrier width, respectively (compare Fig. 11). Here we assume that the applied voltage U drops symmetrically over the two barriers alone, i.e., we neglect any voltage drop within the heavily doped *a*-Si:H layers. When these energies are added to the configuration energy diagrams as in Fig. 10 they reproduce the changes in time constants as reported in Figs. 9(a) and 9(b).

Let us suppose for illustrative purposes that the trap is situated close to the downstream (i.e., the right-hand side in Fig. 11) *a*-Si:H layer and let us further assume that charge exchange proceeds via tunneling between the localized trap state and the *a*-Si:H conduction-band states. This will strongly favor charge exchange with the nearest

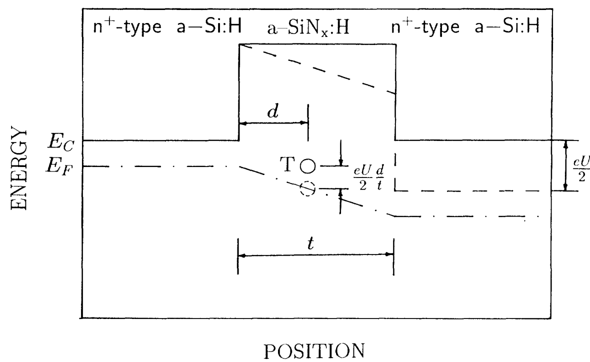

FIG. 11. Band diagram for one of the two barriers with and without an externally applied voltage U.

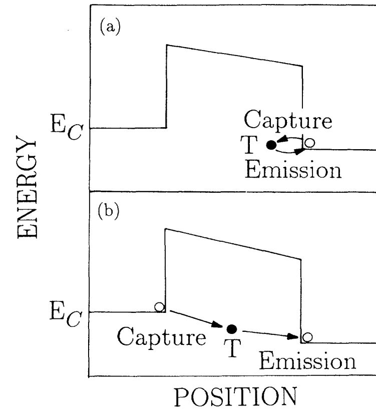

FIG. 12. Possible capture and emission processes for a trap T situated in a nitride layer: (a) capture and emission to the same *a*-Si:H layer; (b) capture from the upstream and emission to the downstream layer. The energy of the trap shifts relative to the conduction-band edges of the adjacent *a*-Si:H layers with a change of the applied voltage.

a-Si:H layer. This situation will thus be as schematically illustrated in Fig. 12(a) and the corresponding configuration energy diagram is shown in Fig. 13 both cases with and without applied voltage.

In order to understand the diagram it is best to use the energy parabola of the filled trap as a reference. The parabola of the empty T^0 *plus* an electron in the *a*-Si:H conduction band is displaced to the left and raised in energy to the binding energy of the electron at the trap. With applied voltage the energy of a conduction electron in the downstream conduction band is *lowered* with respect to the trap energy level (compared Fig. 11) and thus the whole trap plus free-electron parabola is displaced down-

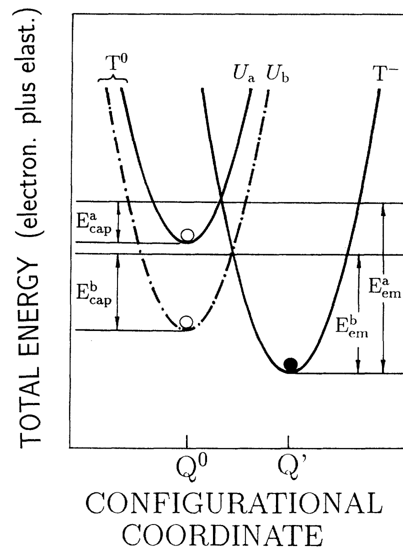

FIG. 13. Relative position of the configuration diagrams for two different applied voltages U_a and U_b. The barriers for capture and emission are influenced by the applied voltage.

TABLE I. Characteristics of RTN for three different traps (T_1-T_3). The capture and emission time constants were determined in the indicated temperature and voltage ranges. ΔE_{cap} and ΔE_{em} refer to the thermal activation energies for the capture ($\bar{\tau}_c$) and emission ($\bar{\tau}_e$) time constants, respectively. Also indicated are the changes of $\bar{\tau}_c$ and $\bar{\tau}_e$ for a change of the voltage U applied to the sample.

Trap	T_1	T_2	T_3
Sample	230-D2	230-D3	230-D2
Temperature range (K)	275...311	228...238	215
Voltage range (V)	0.79	0.08...0.20	1.125...1.50
	0.72±0.05	0.40±0.07	
	(U=0.79 V)	(U=0.08 V)	
ΔE_{cap} (eV)		0.41±0.05	
		(U=0.12 V)	
		0.43±0.06	
		(U=0.20 V)	
	0.87±0.05	0.44±0.07	
	(U=0.79 V)	(U=0.08 V)	
ΔE_{em} (eV)		0.43±0.05	
		(U=0.12 V)	
		0.41±0.06	
		(U=0.20 V)	
$\bar{\tau}_c$ for increasing voltage U		increases	decreases
$\bar{\tau}_e$ for increasing voltage U		decreases	decreases

wards by the same amount.

By comparing the configurational barriers one can see that the barrier for capture is raised and that for emission is lowered upon applying a voltage to the barrier structure. The capture and emission time constants are thus expected to decrease and increase, respectively, as well. This is indeed observed for trap T_2 [compare Fig. 9(a)] and can be traced to the corresponding changes in the thermal activation energies (see Table I). The complementary situation holds for charge exchange with the upstream conduction band. A *counteracting* change in time constants with applied voltage is thus the *normal* state of affairs for our kind of device.

A special situation may occur in those rare instances when the trap is placed close to the center of the barrier layer such that the tunneling rates to or from either of the two *a*-Si:H layers are equal. Then the situation schematically shown in Fig. 12(b) might occur, namely that the trap is charged from the upstream and discharges into the downstream layer. An analogous evaluation of the configuration energy diagram (compare Fig. 13) yields that *both* barriers decrease with increasing applied voltage, a behavior obviously observed for trap T_3.

As mentioned above the effect of light on the occupation statistics of the trap responsible for RTN offers access to the microscopic mechanism of charge exchange at individual traps. Starting illumination of the sample with light intensities smaller than those used in Fig. 5, i.e., with 1.3×10^8 photons s^{-1} μm^{-2} we find that $\bar{\tau}_e$ decreases with increasing light intensity until the RTN disappears while $\bar{\tau}_c$ remains nearly unaffected (compare Fig. 14). Illumination of the sample generates a nonequilibrium carrier distribution. The quasi-Fermi level for electrons shifts (locally) to the conduction-band edge and that of the holes towards the valence-band edge. This means for the defect-controlling trap state that its capture time constant $\bar{\tau}_c$ is expected to decrease as additional electrons for defect occupation are generated by illumination. However, since the net photocurrent which serves as a measure for the excess photogenerated carriers is less than 1% of the total current through the device (compare Fig. 7) the capture time constant $\bar{\tau}_c$ is only little affected. To explain the decrease of the emission time constant $\bar{\tau}_e$ a direct optical excitation from the defect or a recombination of the defect charge with photogenerated holes

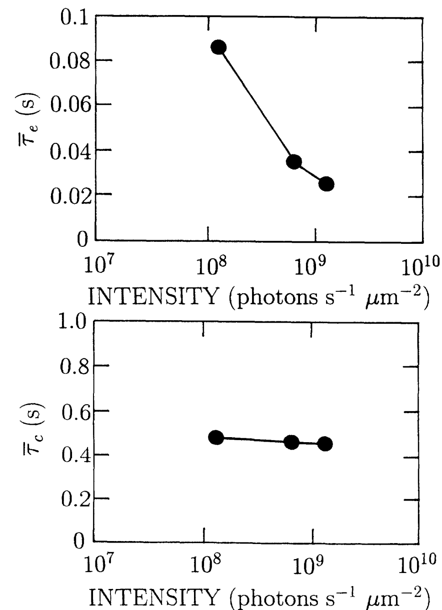

FIG. 14. Dependence of the emission ($\bar{\tau}_e$) and capture ($\bar{\tau}_c$) time constants of trap T_1 on illumination intensity. The laser was focused on the light-sensitive area. The lines connect the experimental points.

has to be considered. We believe that the second alternative is more likely for the following reason. For a direct optical excitation with an intensity that suffices to quench the RTN we expect a return of the RTN immediately after the end of illumination. This is not observed. Because of the n^+-type doping of the a-Si:H layers and the large band gap of the nitride barriers the hole concentration for a defect recombination is negligible without illumination. By optical excitation of electrons from the a-Si:H valence band a high hole concentration is generated locally. Holes can tunnel into the nitride layer to recombine with the trap charge. The second alternative can also explain the behavior of the sample noise at the end of the illumination when the net photo current decays exponentially in time with a time constant of the order of a second. Only if the local hole concentration near the trap falls below a threshold value does the RTN set in again.

ACKNOWLEDGMENTS

Early parts of this work were done at the Max-Planck-Institut für Festkörperforschung, Heisenbergstraße 1, 7000 Stuttgart 80, FRG. One of us (R.A.) thanks the Alexander-von-Humboldt-Stiftung for support. Parts of this work were supported by the Bundesministerium für Forschung und Technologie under Contract No. 0328962A.

[1]D. Wolf and E. Holler, J. Appl. Phys. **38**, 189 (1967).

[2]B. Neri, P. Olivo, and B. Ricco, Appl. Phys. Lett. **51**, 2167 (1987).

[3]R. E. Cavicchi and M. B. Panish, J. Appl. Phys. **67**, 873 (1990).

[4]C. T. Rogers and R. A. Buhrman, Phys. Rev. Lett. **53**, 1272 (1984).

[5]C. T. Rogers, K. R. Farmer, and R. A. Buhrman, in *Proceedings of the 9th International Conference on Noise in Physical Systems,* edited by C. M. Van Vliet (World Scientific, Singapore, 1987), p. 293.

[6]M. E. Welland and R. H. Koch, Appl. Phys. Lett. **48**, 724 (1986).

[7]A. D'Amico, G. Fortunato, and C. M. Van Vliet, Solid-State Electron. **28**, 837 (1985).

[8]C. T. Rogers, R. A. Buhrman, H. Kroger, and L. N. Smith, Appl. Phys. Lett. **49**, 1107 (1986).

[9]W. K. Choi, A. E. Owen, P. G. LeComber, and M. J. Rose, J. Appl. Phys. **68**, 120 (1990).

[10]C. E. Parman, N. E. Israeloff, and J. Kakalios, Phys. Rev. B **44**, 8391 (1991).

[11]K. S. Ralls, W. J. Skocpol, L. D. Jackel, R. E. Howard, L. A. Fetter, R. Epworth, and D. M. Tennant, Phys. Rev. Lett. **52**, 228 (1984).

[12]R. E. Howard, W. J. Skocpol, L. D. Jackel, P. M. Mankiewich, L. A. Fetter, D. M. Tennant, R. Epworth, and K. S. Ralls, IEEE Trans. Electron. Devices **ED-32**, 1669 (1985).

[13]M. J. Uren, D. J. Day, and M. J. Kirton, Appl. Phys. Lett. **47**, 1195 (1985).

[14]M. J. Kirton and M. J. Uren, Appl. Phys. Lett. **48**, 1270 (1986).

[15]M. J. Kirton, M. J. Uren, and S. Collins, Appl. Surf. Sci. **30**, 148 (1987).

[16]M. Bollu, F. Koch, A. Madenach, and J. Scholz, Appl. Surf. Sci. **30**, 142 (1987).

[17]P. Restle, Appl. Phys. Lett. **53**, 1862 (1988).

[18]M. J. Kirton, M. J. Uren, S. Collins, M. Schulz, A. Karmann, and K. Scheffer, Semicond. Sci. Technol. **4**, 1116 (1989).

[19]M. J. Kirton and M. J. Uren, Adv. Phys. **38**, 368 (1989).

[20]A. Ohata, A. Toriumi, M. Iwase, and K. Natori, J. Appl. Phys. **68**, 200 (1990).

[21]K. R. Farmer, C. T. Rogers, and R. A. Buhrman, Phys. Rev. Lett. **58**, 2255 (1987).

[22]R. Arce and L. Ley, in *Amorphous Silicon Technology,* edited by A. Madan, M. J. Thompson, P. C. Taylor, Y. Hamakawa, and P. G. LeComber, MRS Symposia Proceedings No. 149 (Materials Research Society, Pittsburgh, 1989), p. 675.

[23]R. Arce, L. Ley, and M. Hundhausen, J. Non-Cryst. Solids **114**, 696 (1989).

[24]F. Evangelisti, J. Non-Cryst. Solids **77&78**, 969 (1985).

[25]M. Hundhausen, P. Santos, L. Ley, F. Habraken, W. Beyer, R. Primig, and G. Gorges, Phys. Rev. Lett. **59**, 125 (1987).

[26]S. Miyazaki, Y. Ihara, and M. Hirose, Phys. Rev. Lett. **59**, 125 (1987).

[27]M. Buckingham, *Noise in Electronic Devices and Systems* (Ellis Horwood, Chichester, 1983).

[28]S. M. Kay and S. L. Marple, Jr., Proc. IEEE **69**, 1380 (1981).

[29]S. Machlup, J. Appl. Phys. **25**, 341 (1954).

[30]M. Lax, J. Appl. Phys. **48**, 3919 (1977).

[31]See, e.g., J. D. Jackson, *Classical Electrodynamics,* 2nd ed. (De Gruyter, Berlin, 1983).

[32]D. T. Krick, P. M. Lenahan, and J. Kanicki, Appl. Phys. Lett. **51**, 608 (1987).

[33]J. Kanicki, D. Jousse, A. Gelatos, and M. S. Crowder, J. Non-Cryst. Solids **114**, 612 (1989).

[34]P. M. Lenahan and D. T. Krick, Appl. Surf. Sci. **39**, 392 (1989).

[35]E. Iborra, J. A. Lopez-Rubio, I. Esquivas, J. Sanz-Maudes, and T. Rodriguez, J. Appl. Phys. **67**, 1617 (1990).

[36]Y. Kamigaki, S. Minami, and H. Kato, J. Appl. Phys. **68**, 2211 (1990).

[37]W. L. Warren, P. M. Lenahan, and S. E. Curry, Phys. Rev. Lett. **65**, 207 (1990).

[38]S. Kanicki and S. Hug, Appl. Phys. Lett. **54**, 733 (1989).

[39]C. H. Henry and D. V. Lang, Phys. Rev. B **15**, 989 (1977).

[40]C. T. Rogers and R. A. Buhrman, Phys. Rev. Lett. **55**, 859 (1985).

[41]A. Karmann and M. Schulz, in *Proceedings of the International Conference on Insulating Films INFOS89,* edited by F. Koch and A. Spitzer (North-Holland, Amsterdam, 1989), p. 500.

[42]J. A. Van Vechten and C. D. Thurmond, Phys. Rev. B **14**, 3539 (1976).